oceans

MDPI

Article

Revisiting Satellite Chlorophyll–*a* Retrievals in the River-Influenced Coastal Upwelling Area off Central-Southern Chile

Gonzalo S. Saldías [1,2], Richard Muñoz [3], Alexander Galán [4,5], Roberto Aedo-Garcia [1], Carlos Lara [6] and Fabián J. Tapia [2,7,*]

[1] Departamento de Física, Facultad de Ciencias, Universidad del Bío-Bío, Concepción 4051381, Chile; gsaldias@ubiobio.cl (G.S.S.); raedogar@ubiobio.cl (R.A.-G.)
[2] Centro de Investigación Oceanográfica COPAS COASTAL, Universidad de Concepción, Concepción 4070386, Chile
[3] Programa de Postgrado en Oceanografía, Universidad de Concepción, Concepción 4070386, Chile; richmunoz@udec.cl
[4] Centro de Investigación de Estudios Avanzados del Maule (CIEAM), Vicerrectoría de Investigación y Postgrado, Universidad Católica del Maule, Talca 3460000, Chile; agalan@ucm.cl
[5] Coastal Social-Ecological Millennium Institute (SECOS), Santiago 8331150, Chile
[6] Departamento de Ecología, Facultad de Ciencias, Universidad Católica de la Santísima Concepción, Concepción 4090541, Chile; carlos.lara@ucsc.cl
[7] Departamento de Oceanografía, Facultad de Ciencias Naturales y Oceanográficas, Universidad de Concepción, Concepción 4070386, Chile
* Correspondence: ftapiaj@udec.cl

Abstract

Satellite chlorophyll–*a* (Chla) products are widely used to study coastal productivity, but their performance often degrades in river-influenced and optically complex waters. We evaluated MODIS-Aqua Chla retrievals in the coastal upwelling area off central-southern Chile, a region strongly affected by seasonal river plumes, using monthly in situ Chla and hydrographic observations from Station 18 (August 2002 to September 2011), daily MODIS products, and matchup analyses based on 3×3 pixel windows and 1-, 3-, 5-, and 7-day composites. MODIS Chla and normalized Fluorescence Line Height (nFLH) reproduced the broad seasonal cycle, with maxima during spring–summer, but default MODIS Chla systematically exceeded in situ observations, particularly during periods of enhanced turbidity and river-influenced optical complexity. Among the raw satellite products, 1-day MODIS Chla matchups showed the strongest agreement with in situ Chla (r = 0.77, RMSE = 8.5 mg m^{-3}), whereas 5-day composites increased matchup availability to 95% but reduced the correlation (r = 0.46, RMSE = 10.5 mg m^{-3}). In contrast, nFLH showed more stable performance across composite lengths, although it underestimated high Chla values and should therefore be interpreted as a complementary fluorescence-based diagnostic rather than as a direct substitute for locally validated Chla retrievals. A gradient boosting model trained with MODIS remote-sensing reflectances improved the correspondence between satellite and in situ Chla relative to the default MODIS product within the available Station 18 matchup dataset. Because this model was evaluated using cross-validation rather than an independent regional validation dataset, the machine-learning results should be interpreted as a local proof of concept rather than a fully validated regional algorithm. These results indicate that standard MODIS algorithms overestimate Chla in this river-influenced upwelling system and highlight the value of local correction approaches, including machine-learning methods, for improving coastal ocean color products, provided that future applications include independent spatially distributed validation and improved bio-optical characterization of river-influenced waters.

Academic Editor: Diego Macías

Received: 23 April 2026
Revised: 25 June 2026
Accepted: 30 June 2026
Published: 13 July 2026

 https://doi.org/10.3390/oceans7040059

Keywords: turbid waters; river plumes; satellite chlorophyll; hydrography; central-southern Chile

1. Introduction

Ocean color remote-sensing is crucial for studying surface ocean processes [1]. Measurements from the Coastal Zone Color Scanner (CZCS), Ocean Color and Temperature Scanner (OCTS), Sea-viewing Wide Field-of-view Sensor (SeaWiFS), Moderate Resolution Imaging Spectroradiometer (MODIS), and Medium Resolution Imaging Spectrometer (MERIS) have estimated surface chlorophyll–*a* (Chla) concentrations from space since the late 1970's [2]. These satellite observations have revealed revolutionary findings primarily on oceanic primary production [e.g., [3–5]]. Although satellite-derived estimates of Chla are generally not as accurate as in situ measurements [e.g., [6]], satellite measurements provide high temporal resolution and global coverage of ocean color fields. In contrast, in situ measurements are commonly limited to either long time series from fixed oceanographic stations or sparse spatial coverage during a short period of time (i.e., shipboard surveys). In fact, in situ measurements of Chla are unevenly distributed across oceanic regions, with most data from Western Boundary Currents and the Equatorial Pacific [7]. Satellite measurements are therefore essential for the study of surface Chla variability over a wider geographic range and at multiple spatio-temporal scales [e.g., [8–16]].

In general, Chla algorithms are based on visible wavelengths. SeaWiFS and MODIS default algorithms rely on bands in the visible and near-infrared spectrum to estimate Chla concentration [17]; however, their performance can vary considerably across regions. The standard Chla algorithms for SeaWiFS (OC4) and MODIS (OC3) use bands centered at 443, 488, and 551 nm [18,19]. Their maximum spatial resolution is conventionally at 1 km; nonetheless, Chla estimates at 500 m have been obtained using the MODIS bands centered at 469 nm and 555 nm [19]. More recently, several studies evaluating Chla retrievals in coastal and inland waters have demonstrated that default empirical and semi-analytical algorithms are highly biased in turbid and optically complex conditions [e.g., [20–24]], which makes it necessary to develop new local algorithms for coastal waters. These biases are particularly important for blue–green band-ratio algorithms such as OC3, which assume that changes in the blue-to-green reflectance ratio are primarily controlled by phytoplankton pigment absorption [25]. In river-influenced waters, this assumption can be violated because colored dissolved organic matter (CDOM) absorbs strongly in the blue bands, while total suspended matter (TSM) and other particles modify scattering and reflectance at green and longer wavelengths [e.g., [26]]. Atmospheric-correction errors can further affect retrievals in turbid coastal waters, especially when the assumption of negligible water-leaving radiance in the near-infrared bands is not satisfied [27,28].

In this context, fluorescence-based satellite products and locally trained correction approaches provide useful complementary tools for evaluating Chla retrievals in optically complex waters [29–32]. Normalized Fluorescence Line Height (nFLH) can provide an independent fluorescence-based indicator of phytoplankton variability, although it is not a direct substitute for extracted or locally validated Chla because fluorescence yield depends on physiological state, light history, non-photochemical quenching, pigment packaging, and community composition [33,34]. Similarly, machine-learning approaches trained with local remote-sensing reflectance and in situ Chla observations may improve correspondence with field data [35], but their predictive skill depends strongly on the validation design and the availability of independent observations. Therefore, machine-learning corrections should be interpreted cautiously when they are developed from limited matchup datasets and evaluated only through cross-validation.

In the last few decades, satellite ocean color algorithms have provided valuable information for monitoring the coastal marine environment along the Chilean coast (18° S–45° S). Using satellite data, [36] characterized the annual cycle of coastal and ocean Chla concentration off Chile (18° S–40° S). Similarly, a marked seasonality in upwelling activity and mesoscale features involving coastal Chla (e.g., cold coastal filaments and eddies) has been documented off central Chile (35° S–38° S) [37,38]. Nevertheless, freshwater discharge from several closely spaced rivers delivers a wide variety of dissolved and particulate constituents into coastal waters, influencing their optics and creating highly turbid conditions [39–41]. In these cases, satellite Chla retrievals could be highly biased due to the presence of colored dissolved organic matter (CDOM), which has a strong absorption in blue bands [42,43], and total suspended matter (TSM) that contributes to scattering at longer wavelengths [44]. In addition, seasonal changes in phytoplankton biomass, community structure, cell size, and pigment composition [38,45–47] may further modify the optical signal in this productive upwelling region. Therefore, to improve the accuracy of satellite-derived Chla estimates, it is necessary to evaluate the remote ocean color signal in the river-influenced coastal ocean off central-southern Chile.

The goal of this study is to provide the first assessment of satellite-derived Chla in the coastal region off central-southern Chile, which is frequently affected by turbid river plumes during fall, winter, and spring. Special attention is given to bias in Chla estimates during periods of increased turbidity. A time series of in situ estimates of Chla and hydrographic measurements is used, in combination with satellite retrievals. We also evaluate MODIS nFLH as a complementary fluorescence-based diagnostic and explore whether a locally trained machine-learning model using MODIS remote-sensing reflectances can improve the correspondence between satellite and in situ Chla at Station 18. Because this machine-learning analysis is based on a limited single-station matchup dataset, it is treated as an exploratory proof of concept rather than a fully validated regional algorithm. Section 2 contains the data and methods. Section 3 presents the main results evaluating the performance of MODIS Chla estimates. The discussion is presented in Section 4, emphasizing the importance of correcting the default algorithms for future studies of coastal Chla variability. Finally, the main conclusions are highlighted in Section 5.

2. Data and Methods

2.1. Study Area

The coastal ocean off central-southern Chile (Figure 1) is one of the most productive regions in the world [48], with high Chla concentrations during the spring–summer upwelling season (Figure 2a,d). Here, both wind-driven coastal upwelling and river discharges exhibit dominant seasonal variability, with greater intensity during spring–summer and winter, respectively [39,49,50]. High freshwater outflow events coincide with strong and frequent upwelling in spring. Moreover, coastal upwelling modulates the annual cycle of satellite-derived Chla [36,51], while mesoscale eddies transport high-biomass waters offshore [52]. In addition, an extended coastal band of high turbidity has been described along central-southern Chile due to the spreading of river plumes [39], which can become anomalously large during warm El Niño phases [40]. These hydrographic and optical conditions are expected to affect the performance of standard satellite Chla retrievals, particularly during winter and spring when turbid outflows are more pronounced (Figure 2). Accordingly, this region provides a suitable natural setting to evaluate whether default MODIS Chla estimates are biased under river-influenced coastal conditions. In fact, the highest satellite Chla values over the shelf are found in spring along the entire coast

(Figure 2d). Although this maximum Chla in the annual cycle is supported by Chla fluorescence, which is not affected by near-surface turbidity, the maximum fluorescence is enhanced in particular locations and not all along the coast (Figure 2h). Furthermore, the peaks in average Chla during fall–winter around the river mouths could also result from an overestimation of satellite-derived Chla in the coastal ocean off central-southern Chile during high-runoff events.

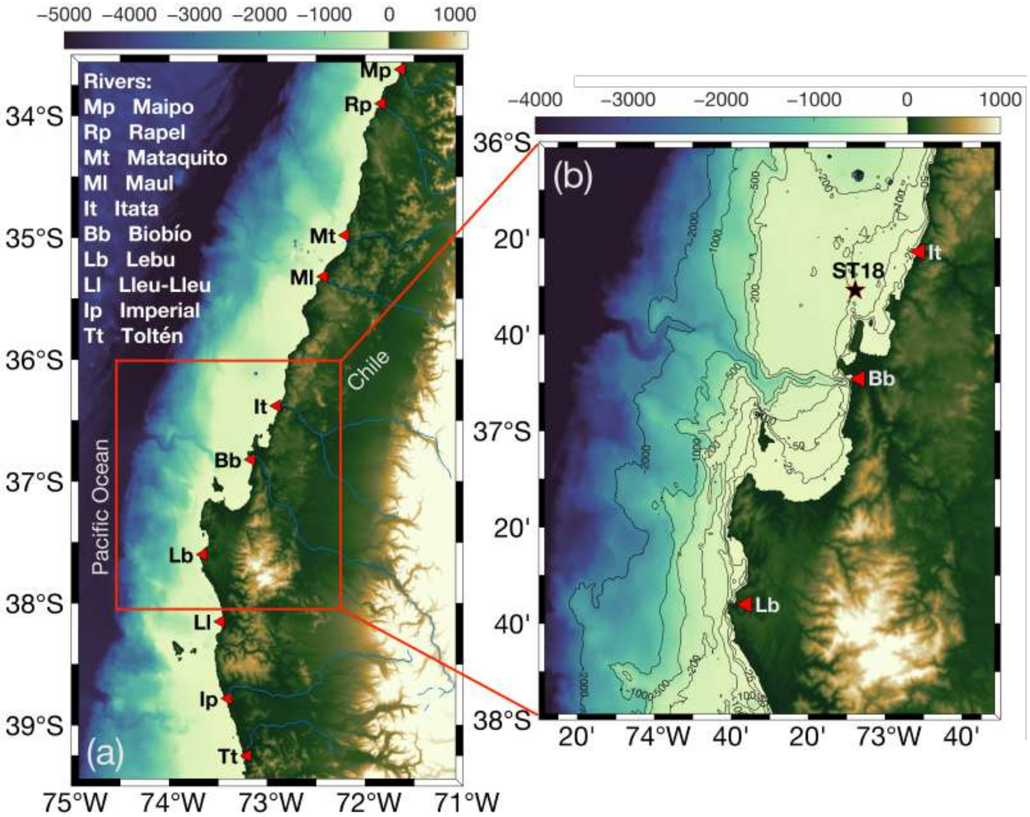

Figure 1. (**a**) River−influenced upwelling region off central−southern Chile. The enclosed coastal ocean off Concepción, where the oceanographic station was located, is presented in (**b**). The positions of the rivers connecting to the coastal ocean are indicated by black triangles. The ocean depth and height of the adjacent landscape are shown in color. The oceanographic station (St18) is presented as a black star over the continental shelf at ∼36.5° S in (**b**).

2.2. Ocean Color Imagery

All daily satellite ocean color data from the Moderate Resolution Imaging Spectroradiometer on Aqua (MODIS-Aqua) were used to generate daily images of near-surface Chla, normalized Fluorescence Line Height (nFLH), and all visible remote-sensing reflectance bands (Rrs(λ)) for the period of July 2002–September 2011. MODIS Level 1 (L1) files were obtained from NASA (https://oceancolor.gsfc.nasa.gov; accessed on 26 January 2021) and processed using the SeaWiFS Data Analysis System (SeaDAS) to produce daily ocean color images at 1 km spatial resolution. A detailed explanation of SeaDAS processing steps for this coastal region is found in [39]. In the present study, MODIS-Aqua Level 1 files were processed using the default NASA/SeaDAS atmospheric-correction configuration, including the standard NIR-based aerosol correction. Alternative SWIR or NIR-SWIR atmospheric correction schemes were not applied here because our objective was to evaluate the standard MODIS Chla product as commonly used in previous regional studies. Standard SeaDAS quality-control flags were used to exclude invalid pixels affected by clouds, land, high glint, atmospheric-correction failure, stray light, or other processing problems before matchup extraction.

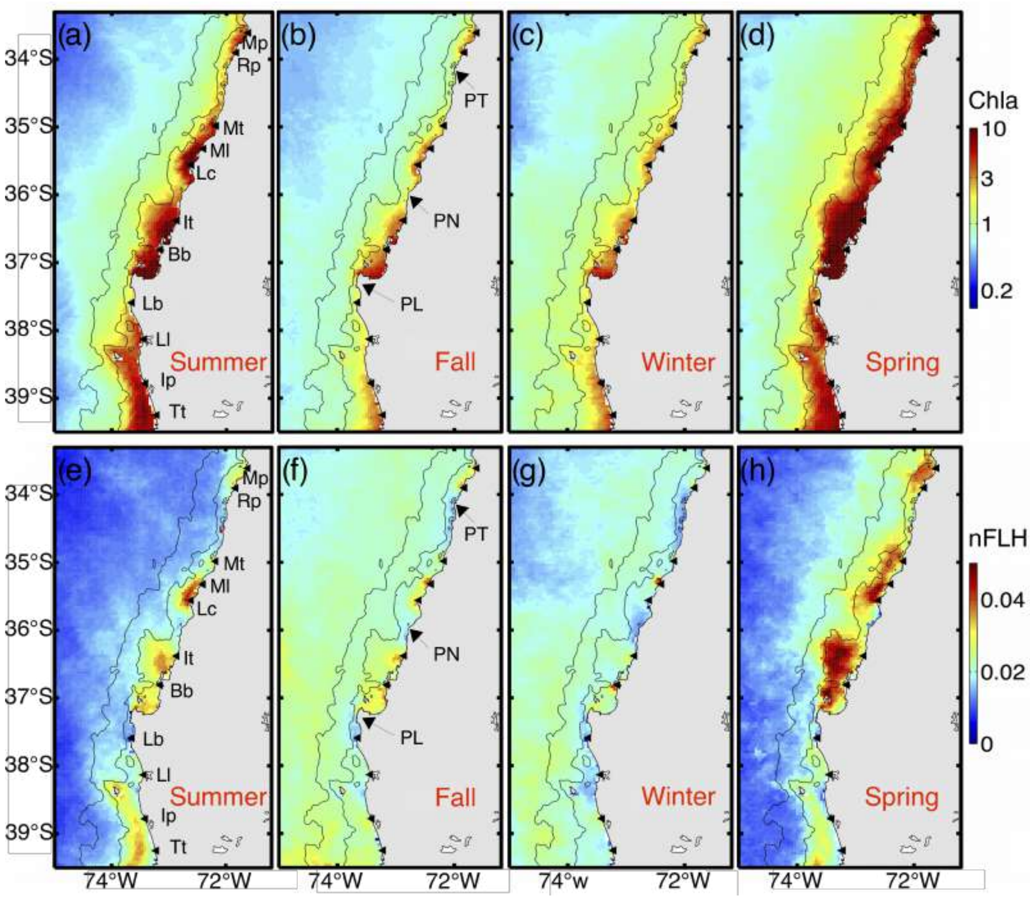

Figure 2. Seasonal variability of MODIS chlorophyll–*a* (Chla, **a**–**d**) and normalized Fluorescence Line Height (nFLH, **e**–**h**) based on four years (2006–2009) of high-resolution MODIS imagery off central-southern Chile. Seasonal averages correspond to (**a**,**e**) summer, (**b**,**f**) fall, (**c**,**g**) winter, and (**d**,**h**) spring.

In coastal turbid waters, the use of default NIR bands for atmospheric corrections may result in substantial errors of final ocean color products [28]. To overcome this issue, the use of SWIR bands (1240 and 2130 nm for MODIS) is recommended because the ocean reflectance values at these bands are close to zero (i.e., stronger water absorption) [53]. In this study, we opted to maintain default settings to account for potential errors in the Chla readings and to compare with results from previous studies. Future efforts will evaluate the effects of contrasting atmospheric corrections on the accuracy of ocean color outputs off the central-southern coast of Chile.

2.3. Time Series Station

A hydrographic station located ∼20 km offshore over the ∼90 m isobath between the Biobio and Itata Rivers (Figure 1) was sampled monthly from August 2002 to September 2011 (with a few gaps due to weather conditions) by the COPAS Oceanographic Research Center at Universidad de Concepción. In each cruise, multiple CTD profiles were conducted during the day to obtain the average vertical structure of hydrographic conditions. In addition, water samples were taken at different depth levels (0, 5, 10, 15, 20, 30, 40, 50, and 80 m) for chemical and biological analyses, including Chla concentrations. For the satellite matchup analysis, the in situ Chla reference was defined as the 0–10 m average Chla because MODIS ocean color retrievals represent the near-surface optical signal. The same near-surface Chla definition was used consistently for all satellite-product comparisons and for the machine-learning target variable. Additional details on these measurements can be found in [47].

2.4. Matchups Extraction and Statistical Analyses

Satellite matchups were generated by averaging a 3 × 3-pixel window centered on the in situ sampling location and applying quality-control procedures following [54], including a comparison with a nearest-neighbor approach to assess spatial homogeneity. Only valid water pixels that passed the SeaDAS quality-control criteria were retained in the 3 × 3 window. Pixels flagged as cloudy, land-contaminated, affected by high glint, atmospheric-correction failure, stray light, or other standard quality-control problems were excluded before averaging. A matchup was retained only when at least 5 of the 9 pixels were valid. To reduce the influence of spatial outliers and land effects, we also used a 2D median filter prior to extraction.

Due to high temporal variability, this average spatial window is recommended for filtering satellite and algorithmic noise [55]. We extracted these matchups using several temporal composites centered on the dates of in situ sampling (Figure 3).

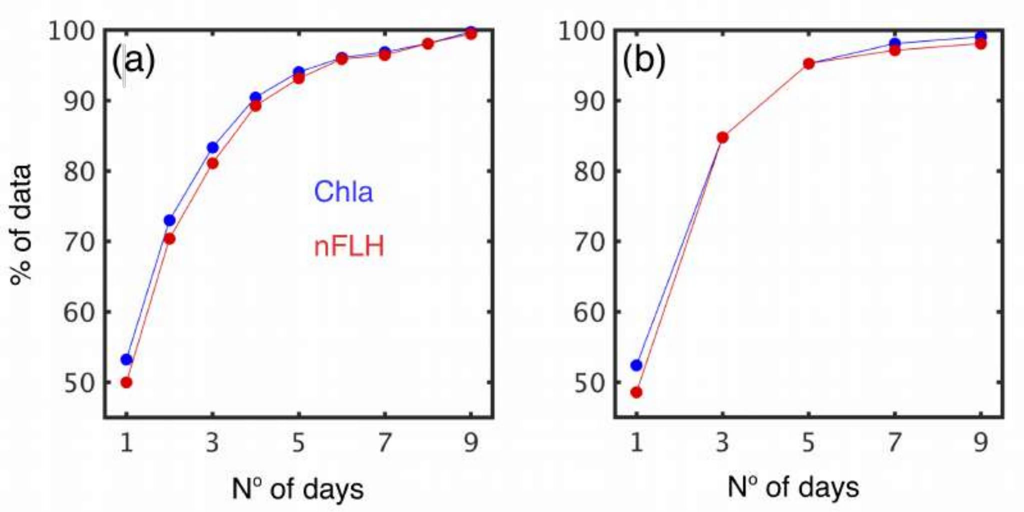

Figure 3. Percentage of cloud-free ocean color data (Chla and nFLH) for a 3 × 3 window centered on the location of Station 18 (see Figure 1) as a function of the number of days used to produce composites for (**a**) all MODIS images available for Aug 2002-Sep 2011, and (**b**) all MODIS composites centered on those days of in situ Chla sampling at Station 18 (% of matchups).

Because exact cruise sampling times were not available for all dates, matchups were based on daily MODIS-Aqua products centered on the in situ sampling date. MODIS-Aqua daytime overpasses in the study region generally occur in the early afternoon, approximately between 14:00 and 15:30 Chilean local time (UTC-4). This temporal mismatch is an additional source of uncertainty in the matchup analysis. The statistical correspondence between in situ and satellite measurements quantifies how well the satellite data represent the observed ocean Chla [56].

We calculated the root mean squared error (RMSE), correlation coefficient (r), *p*-value, and other statistics to evaluate the relationship between satellite composites (1, 3, 5, and 7 days) and the in situ measurements. Because the default MODIS Chla product showed systematic positive deviations relative to the in situ observations, we also calculated additional error metrics, including bias, median error, mean absolute error (MAE), relative error, and log-transformed error metrics. These metrics were used to better quantify both the direction and magnitude of the retrieval errors. A linear regression model was fitted to obtain the slope and intercept of the relationship between the measurements.

We also performed a preliminary analysis of machine-learning models to explore whether machine-learning models could improve the relationship between satellite and in situ data [57,58]. Different methods were evaluated considering all MODIS remote-sensing reflectances (412–678 nm) as predictor variables and in situ Chla as the target variable. The tested algorithms included GBM, GBM with cross-validation, stacked ensemble, multilayer perceptron, and extremely randomized trees. GBM showed the best overall performance in terms of RMSE and MSE, with MAE values comparable to the best-performing models. The model selection was based only on the training–validation workflow to avoid using the full dataset for model optimization. To mitigate the problems associated with a limited number of matches, cross-validation techniques were applied to train the model, assess its performance, and compensate for the relatively small amount of data [59]. No fully independent spatial or temporal validation dataset was available for the present study. Therefore, the machine-learning results should be interpreted as an exploratory assessment based on cross-validation within the Station 18 matchup dataset. Future applications should evaluate temporally blocked or year-grouped validation schemes, as well as independent validation at additional coastal stations, before the model can be generalized regionally.

Prior to model training, missing values in the MODIS remote-sensing reflectances (Rrs) were completed through an imputation procedure to preserve the largest possible number of valid matchups and retain full spectral information. Missing Rrs values were completed using a regression-based imputation approach, in which missing values in each spectral band were estimated from the remaining available MODIS Rrs predictors. Unlike the standard MODIS chlorophyll product, which is based on a reduced set of spectral relationships, the machine-learning approach used here incorporated all available MODIS reflectance bands (412, 443, 469, 488, 531, 547, 555, 645, 667, and 678 nm) as predictor variables. Several machine-learning algorithms were tested during the exploratory stage, and the final model selected for Chla prediction was a Gradient Boosting Machine (GBM), which showed the best overall performance in reproducing the in situ observations [60–62].

The machine-learning analysis was restricted to predicting in situ Chla from MODIS remote-sensing reflectance bands. MODIS nFLH was not used as a target variable or incorporated into the machine-learning correction because no independent in situ fluorescence or nFLH validation dataset was available for the study period. Therefore, nFLH was analyzed only as a complementary satellite-derived diagnostic to evaluate whether a fluorescence-based product exhibited behavior consistent with or distinct from that of the standard MODIS Chla product.

3. Results

3.1. Seasonal Evolution of Chla, nFLH, and Surface Hydrography

Satellite fields of Chla and nFLH provide a basic description of biological properties in coastal waters off central-southern Chile. Substantial seasonal and spatial variability in Chla and nFLH is observed along the coastal ocean off central-southern Chile. The highest Chla values were observed during austral spring and summer, especially near river mouths, with values > 5 mg m^{-3} (Figure 2a,d). In the austral fall and winter, the Chla was considerably lower than in spring–summer, and the maximum values were found in the region between Punta Lavapie and Punta Nugurne (Figure 2b,c). In contrast to Chla, the seasonal cycle of nFLH shows higher values in spring and considerably lower fluorescence in summer (Figure 2e,h). The highest nFLH values were limited to the areas off the rivers Maipo, Mataquito, Maule, Itata, and Biobio, and primarily in spring (Figure 2h). It is worth noting the large spatial differences between high-Chla and high-nFLH, as well as the relatively low-nFLH in high-Chla regions.

The average surface (top 10 m) hydrographic conditions at Station 18 show a marked seasonal pattern. The 2002–2011 climatology of temperature and salinity shows a cooler and fresher upper ocean in winter (Figure 4a). Similarly, both in situ and satellite Chla, as well as nFLH, exhibited a seasonal cycle with maximum values during spring–summer. However, satellite-derived Chla was consistently higher than the in situ climatology (Figure 4b). The discrepancy was most pronounced from September to May and reached its clearest monthly expression in September, when mean in situ Chla was approximately 3 mg m^{-3}, whereas mean MODIS Chla was approximately 17 mg m^{-3}, equivalent to an overestimation of about 5.7 times. In contrast, both estimates were more similar during winter (July–August).

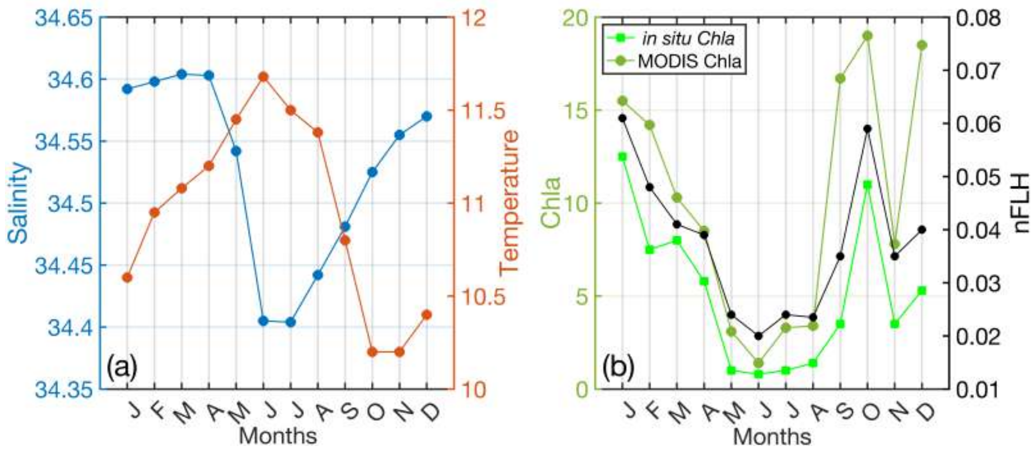

Figure 4. (**a**) Monthly averages for salinity (blue line) and temperature (orange line) integrating the top 10 m of water column at Station 18 (August 2002 to September 2011). (**b**) Monthly averages for MODIS and in situ Chla (green lines) as well as MODIS nFLH (black line) at Station 18.

3.2. Characterization of Matchups and Data Distribution

A composite analysis of matchups, using an increasing number of days to average the satellite window (1-day to 9-day), was conducted to increase the percentage of concomitant observations. The percentage of average satellite Chla values increased from 52% (1-day composites) to 99% (9-day composites) of available cloud-free data at Station 18. nFLH composites showed a similar pattern of available cloud-free information (Figure 3a). MODIS Chla and nFLH increased similarly from ∼50 % (1-day) to 98 % (9-day) of cloud-free data when using composites centered on the dates of available in situ data (Figure 3b). It should be noted that using 5-day MODIS composites increased the % of concomitant (satellite and in situ) observations to 95 % around Station 18. The final number of valid matchups used in the statistical comparisons is reported in Table 1 for each temporal composite. These sample sizes are essential for interpreting the statistical significance and robustness of the reported correlations, RMSE values, and regression parameters.

The distributions of MODIS Chla and nFLH relative to in situ Chla data are presented in Figure 5. The dispersion of MODIS versus in situ Chla data increased from 1-day to 7-day matchup composites, especially during austral spring (red circles) and summer (blue circles). In general, the highest correlation between MODIS Chla and in situ Chla was observed with 1-day MODIS data, and decreased towards the 7-day composites (Figure 5a–d). Additionally, starting with 3-day composites, MODIS Chla tends to overestimate the measured values, with most points above the 1:1 line. In comparison, the dispersion between MODIS fluorescence and in situ Chla is smaller, and the use of composites with several days increased the correlation (Figure 5e–h). A summary of the error statistics and correlation coefficients for these relationships is presented in Table 1. Although correlations were significant, MODIS Chla showed systematic positive deviations relative to in situ values, particularly at moderate to high concentrations. The 1-day matchups showed the best performance ($r = 0.77$, RMSE = 8.5 mg m^{-3}). Lower correlation coefficients and higher RMSE values were observed for the 3-, 5-, and 7-day composites, which represent the highest values of cloud-free days. The use of composites with an increasing number of days increased the correlation between in situ Chla and nFLH, suggesting a more stable relationship between the fluorescence-based product and near-surface Chla variability (Table 1).

Table 1. Statistical summary between in situ Chla and MODIS-derived Chla and nFLH. The parameters shown are the correlation coefficient (r), intercept (a), slope (b), Root Mean Square Error (RMSE), bias, Median signed error (MedE), mean absolute error (MAE), Relative Error (RE), $\log_{10}$ median signed error (LogMedE), *p*-value, and the number of matchups. Error metrics are reported for MODIS Chla only because nFLH is a fluorescence-based product with different units and is evaluated here only as a complementary diagnostic.

Variable	Metric	1 Day	3 Days	5 Days	7 Days
Chla	r	0.77	0.35	0.46	0.26
	a	−0.760	5.921	5.585	8.163
	b	1.488	0.615	0.703	0.532
	RMSE	8.52	12.95	10.51	14.83
	Bias	1.74	3.81	4.03	5.77
	MedE	0.50	0.66	1.11	1.14
	MAE	3.86	6.55	6.72	8.40
	RE (%)	56.91	219.18	232.14	524.40
	LogMedE	0.09	0.18	0.23	0.28
	p-value	9.65×10^{-12}	9.53×10^{-4}	2.29×10^{-6}	6.01×10^{-4}
	Matchups	54	88	99	102
nFLH	r	0.40	0.52	0.50	0.52
	a	0.028	0.028	0.029	0.030
	b	0.001	0.002	0.001	0.001
	p-value	3.48×10^{-3}	2.01×10^{-7}	1.29×10^{-7}	2.20×10^{-8}
	Matchups	50	88	99	101

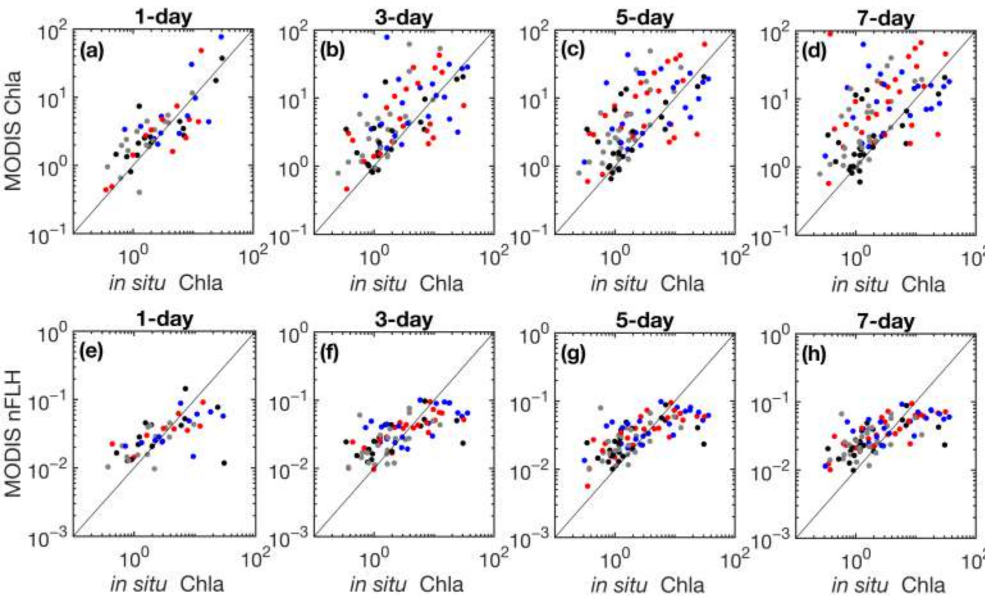

Figure 5. Scatter plots between (top panels) in situ Chla and MODIS Chla, and (bottom panels) in situ Chla and MODIS nFLH, for MODIS composites of (**a**,**e**) 1, (**b**,**f**) 3, (**c**,**g**) 5, and (**d**,**h**) 7 days centered on the dates of in situ measurements. The data are color-coded by season: summer (JFM) in blue, fall (AMJ) in black, winter (JAS) in gray, and spring (OND) in red. A 1:1 straight line is shown in all plots to better visualize the relationship between in situ and satellite data.

To illustrate the frequency distribution of co-located in situ and MODIS data, histograms are presented in Figure 6. Despite the higher correlation between MODIS Chla and in situ Chla when using 1-day matchups (Table 1), there is a clear overestimation of

MODIS Chla, especially for values > 2 mg m^{-3} (Figure 6a). The distribution of matchups does not improve considerably when using composites with a greater number of days; however, the general shape of the 5-day MODIS Chla is closer to the in situ data (Figure 6c). Frequency distributions for MODIS nFLH data (1- to 5-day composites) showed greater resemblance to in situ Chla in the mid to low range (Figure 6e–g), with a clear underestimation towards high in situ Chla values (Figure 6e–h).

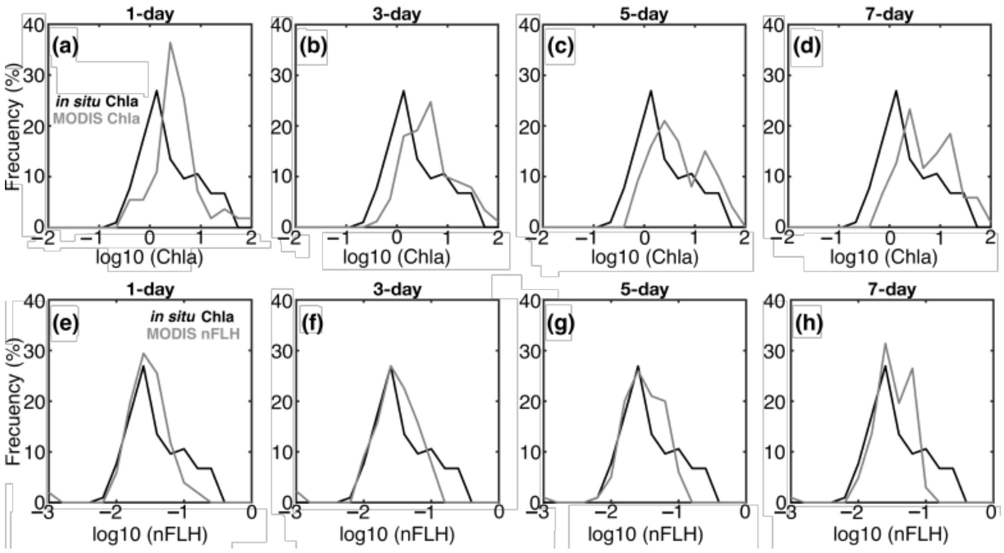

Figure 6. Distribution of (top panels) in situ Chla and MODIS Chla, and (bottom panels) in situ Chla and MODIS nFLH, for MODIS composites of (**a**,**e**) 1, (**b**,**f**) 3, (**c**,**g**) 5, and (**d**,**h**) 7 days centered on the dates of in situ measurements. The change in the x-axis range for the bottom panels was intended to facilitate comparison between the in situ Chla distribution and the nFLH curves.

Table 2 summarizes the performance of the five best machine-learning models. GBM with cross-validation achieved the best overall performance in RMSE and MSE, with MAE values comparable to those of the best-performing models. Additional performance metrics, including bias, median error, relative error, and log-transformed error, are now included to better quantify the systematic differences between satellite-derived and in situ Chla. The GBM model was trained using all available MODIS remote-sensing reflectance bands to generate the model-based Chla product (Figure 7), and compared with MODIS Chla and in situ values. The GBM predictions showed a closer correspondence to the in situ observations than the default MODIS Chla product in the available matchup dataset. This behavior was evident in both linear and log10 space, where the model-based estimates showed reduced dispersion and closer alignment with the fitted regression line. This improvement should be interpreted as an indication that the combined use of MODIS remote-sensing reflectances has potential for local correction of Chla retrievals in this optically complex coastal environment, rather than as evidence of a fully validated regional algorithm.

The temporal comparison in Figure 8 is consistent with the improved correspondence obtained by the model-based Chla product within the available matchup dataset. Although MODIS Chla reproduces part of the observed variability, its time series departs more strongly from the in situ record and tends to show larger mismatches during several peak events. In contrast, the GBM-derived Chla series more closely follows the magnitude and timing of the in situ fluctuations throughout the Station 18 record, yielding a better representation of both background conditions and bloom periods. Some discrepancies remain, particularly at extreme peaks, but the model-based product generally reduces the mismatch compared with the default MODIS estimates. Overall, these results indicate that the GBM approach provides a promising local correction within the Station 18 matchup dataset, but additional independent validation is required before the model can be generalized beyond the Concepción shelf area.

Table 2. Performance metrics (rows) for the selected machine-learning models (columns). RMSE is the Root Mean Square Error, MSE is the mean square error, MAE is the mean absolute error, and RMSLE is the root mean square logarithmic error. Bias corresponds to the mean signed error, MedE to the median signed error, and RE to the relative error expressed as a percentage. LogBias, LogMedE, LogMAE, and LogRMSE are the corresponding error metrics computed in $\log_{10}$ space. Positive values of Bias, MedE, LogBias, and LogMedE indicate overestimation relative to the in situ Chla observations, whereas negative values indicate underestimation.

Statistic	GBM CV	GBM	Stacked Ensemble	MLP	XRT
RMSE	5.130	5.586	5.603	5.628	5.647
MSE	26.319	31.201	31.399	31.669	31.892
MAE	3.227	3.310	3.527	3.465	3.209
RMSLE	0.571	0.525	0.845	0.668	0.344
Bias	0.504	0.807	−2.170	−1.440	0.142
MedE	−0.060	0.645	−0.701	−0.900	0.396
RE (%)	85.884	119.308	154.609	118.698	66.729
LogBias	−1.065	0.151	−2.171	−3.044	0.089
LogMedE	−0.010	0.097	−0.061	−0.187	0.127
LogMAE	1.352	0.308	2.386	3.180	0.206
LogRMSE	3.156	0.369	4.420	5.232	0.258

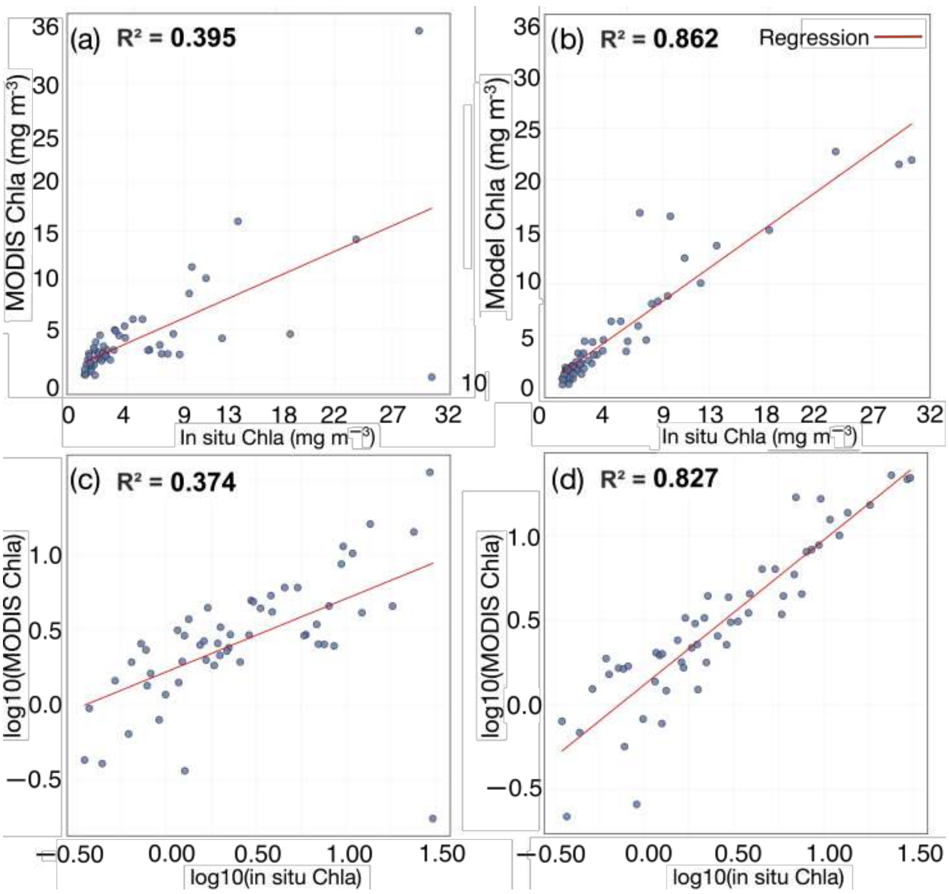

Figure 7. Comparison between in situ Chla and satellite- or model-derived Chla at Station 18. Panels (**a**,**b**) show linear-scale scatterplots of in situ Chla versus MODIS Chla and GBM-predicted Chla, respectively. Panels (**c**,**d**) show the same relationships in log10 space. Red lines indicate linear regressions. The GBM model, trained with MODIS remote-sensing reflectances, shows closer agreement with in situ Chla than the default MODIS product.

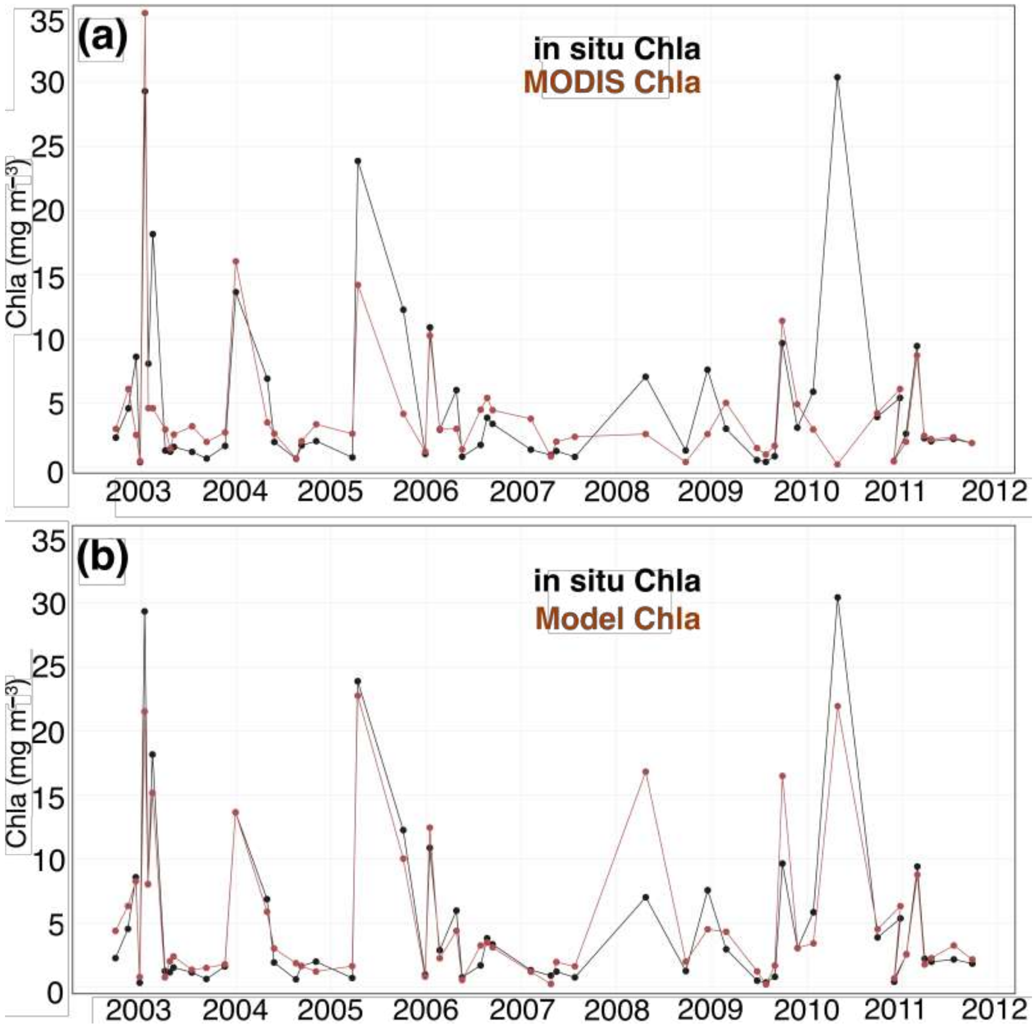

Figure 8. Time series of Chla at Station 18 for August 2002 to September 2011. Black circles/lines denote in situ Chla, whereas red circles/lines correspond to (**a**) MODIS Chla and (**b**) GBM-predicted Chla.

4. Discussion

Despite the limited availability of long in situ Chla records in many coastal regions, several studies have evaluated and corrected satellite Chla retrievals in optically complex waters [6,7,9,14,43]. This need is particularly evident in river-influenced coastal environments, where suspended sediments and colored dissolved material can alter reflectance and reduce the accuracy of standard ocean color algorithms. Along central-southern Chile, turbid river plumes have been clearly identified in MODIS imagery [39–41], yet studies of Chla variability and primary productivity in this region have often relied on default satellite products because of the scarcity of local validation data [13,38,51,63,64]. Using a relatively long in situ time series from Station 18, this study provides a first local assessment of the performance of default MODIS Chla retrievals in a river-influenced upwelling system where both biological variability and water optical properties change markedly through the year.

The agreement between satellite and in situ Chla varied seasonally, with the largest mismatch occurring during spring, particularly in September, when climatological MODIS Chla (∼17 mg m^{-3}) greatly exceeded the in situ mean (∼3 mg m^{-3}). This seasonal decoupling is consistent with the study area's optical complexity. River discharge is enhanced from late fall to early spring, increasing turbidity and modifying surface reflectance through suspended matter and colored dissolved material [39–41], while upwelling-driven variability modulates hydrography and phytoplankton biomass [36,51,52]. In the Concepción shelf system, Chla, cell abundance, and biomass generally peak during spring–summer [64–66], despite short-term intraseasonal variability associated with upwelling intermittence [66]. During this period, the phytoplankton assemblage is commonly dominated by neritic, chain-forming diatoms, whereas in fall–winter, abundance is lower and the community remains diatom-dominated but with a greater contribution from pennate coastal forms [37,64,65,67]. Together, these seasonal changes in hydrography, turbidity, and phytoplankton structure provide a plausible explanation for the reduced performance of the default MODIS Chla product, particularly during spring and other periods of strong river influence. Thus, the observed overestimation should not be interpreted as the result of turbidity alone, but rather as the combined effect of river-derived optical constituents, atmospheric-correction uncertainty, and seasonal biological variability. In particular, changes in phytoplankton community composition, cell size, pigment packaging, and fluorescence yield may also modify the relationship between extracted Chla, reflectance, and fluorescence-based satellite products [45,63,64].

The proposed link between MODIS Chla error and river-influenced optical conditions is also consistent with the hydrographic context at Station 18. Lower near-surface salinity during late fall, winter, and early spring indicates stronger freshwater influence, which coincides with the seasonal development of turbid plumes previously described for the central-southern Chilean coast [39–41]. Because long-term in situ measurements of turbidity, CDOM, and suspended particulate matter were not available for the complete Station 18 record, salinity has been used as an indirect hydrographic proxy for river influence, which is well correlated with surface turbidity in this area [39,40]. This limitation prevents a complete separation of the relative contributions of CDOM, suspended particles, phytoplankton community structure, and atmospheric-correction errors to the MODIS bias. Nevertheless, the seasonal coincidence among fresher surface waters, known regional plume development, and enhanced MODIS Chla overestimation supports the interpretation that river-influenced optical complexity substantially contributes to the observed retrieval errors. Future work should include direct bio-optical measurements, including CDOM absorption, suspended particulate matter, turbidity, particle backscattering, and hyperspectral Rrs, to quantify the mechanisms responsible for the satellite bias more directly.

The matchup analysis also revealed an important tradeoff between data availability and product performance. Short composites yielded the strongest correspondence between MODIS Chla and in situ observations, whereas longer composites substantially increased the number of cloud-free matchups but reduced the agreement with measured Chla. In particular, the 1-day composite produced the highest correlation and lowest RMSE for MODIS Chla, while 5-day composites increased the number of concomitant observations to nearly complete coverage around Station 18. This suggests that temporal averaging improves data availability in this cloudy coastal environment, but at the cost of smoothing short-term biological and optical variability that is likely important in this upwelling system. In contrast, nFLH showed a more stable relationship with in situ Chla across composite lengths and a better frequency distribution for 1- to 5-day composites, although it tended to underestimate high Chla values. These results indicate that nFLH may be a useful complementary indicator of phytoplankton variability in this region, but not a direct substitute for locally validated Chla estimates.

The behavior of nFLH provides additional insight into the region's optical complexity. In contrast to the standard Chla product, nFLH showed a more stable relationship with in situ Chla across composite lengths and a frequency distribution that more closely resembled the in situ data at low to moderate Chla values. This behavior suggests that nFLH may be less sensitive than the standard blue-green Chla algorithm to some river-plume optical effects [e.g., [31]]. However, nFLH underestimated high Chla conditions, indicating that it should not be interpreted as a direct substitute for locally validated Chla retrievals. This underestimation may reflect the nonlinearity of fluorescence at high biomass, physiological variability in fluorescence yield, non-photochemical quenching, pigment packaging, and changes in phytoplankton community composition [e.g., [38,45,68]]. In highly productive coastal systems, fluorescence is not controlled only by pigment concentration, but also by light history, nutrient status, species composition, and photoacclimation [e.g., [69]]. Therefore, the more stable behavior of nFLH at low to moderate Chla values does not imply that it can fully resolve bloom conditions or replace extracted Chla measurements. Instead, nFLH should be used as a complementary diagnostic for identifying phytoplankton-related optical variability and for evaluating whether high MODIS Chla values are consistent with an independent fluorescence-based signal [e.g., [30]].

The reduced performance of the standard MODIS Chla product can be attributed to the spectral assumptions underlying the OC3 blue–green band-ratio algorithm. This algorithm relies on the relationship between Chla concentration and the blue-to-green reflectance ratio, implicitly assuming that phytoplankton pigment absorption is the dominant driver of spectral variability [14]. In river-influenced coastal waters, this assumption can break down because colored dissolved organic matter strongly absorbs in the blue bands, while suspended particulate matter modifies scattering and reflectance at green and longer wavelengths [70]. As a result, changes in the spectral shape caused by river-derived optical constituents may be interpreted by the standard algorithm as increased Chla, producing positive biases even when the signal is not exclusively biological [22]. Atmospheric-correction uncertainties in turbid waters may further amplify these errors because the assumption of negligible water-leaving radiance in the NIR bands is less robust in river plumes [39,71]. Therefore, the MODIS Chla bias observed at Station 18 likely reflects both bio-optical algorithm limitations and uncertainty introduced during atmospheric correction. Testing alternative SWIR or NIR-SWIR atmospheric-correction schemes, together with local bio-optical algorithms, should be a priority for future work in this region.

The machine-learning analysis further suggests that local correction approaches can improve satellite-based Chla retrievals in optically complex coastal waters, in agreement with studies elsewhere [57,58]. Among the evaluated models, the Gradient Boosting Machine (GBM) showed the best statistical performance and produced Chla estimates that were more consistent with the in situ observations than the default MODIS product within the available matchup dataset. However, because the available dataset lacks an independent regional validation set, the machine-learning results should be interpreted with caution. Cross-validation provides a useful initial assessment when sample size is limited, but it cannot fully assess the model's spatial and temporal transferability. Therefore, the GBM product is best regarded as a proof of concept demonstrating that local correction approaches may improve the correspondence between satellite reflectance and in situ Chla at Station 18. Future work should test this approach using independent bio-optical observations from additional coastal stations, ship surveys, and contrasting river-discharge conditions. In the same way, the present analysis retained the default atmospheric-correction settings for MODIS in order to benchmark the standard product against in situ observations; future work should test whether alternative atmospheric-correction schemes further improve retrieval performance in these turbid coastal waters.

The seasonal and interannual dependence of retrieval errors also requires further evaluation. The largest discrepancies are expected during periods when river discharge, turbidity, and biological variability interact, particularly from late winter to spring [46,72–74]. In addition, previous satellite analyses have shown that turbid river plumes off central-southern Chile can expand during anomalous climate conditions, including warm El Niño phases [40]. Because the present validation is based on a monthly time series from a single station, the available matchups are insufficient to fully test the stability of the GBM model across seasons, turbidity regimes, and climate events. Future studies should therefore evaluate model performance using seasonally stratified validation, turbidity classes, and independent observations collected during contrasting discharge and climate conditions. Such an approach would help determine whether locally tuned correction schemes remain stable across different optical regimes or whether separate seasonal, hydrographic, or turbidity-dependent algorithms are required.

More broadly, our results show that default MODIS Chla captures the broad seasonal cycle off central-southern Chile, but systematically overestimates in situ Chla under river-influenced conditions. Because the validation presented here is based on a single monthly time series station, these conclusions are robust for the Concepción shelf area but should not yet be generalized to the entire region off central-southern Chile. Future work should combine spatially distributed bio-optical observations, in situ Chla measurements, and improved atmospheric-correction strategies to develop and validate a regionally tuned coastal Chla algorithm. In this context, machine-learning methods trained with local observations appear to be a promising tool for reducing retrieval bias and improving satellite monitoring of phytoplankton variability in river-influenced upwelling systems. However, any machine-learning-based regional Chla algorithm will require independent spatially distributed validation before it can be used operationally or generalized beyond the shelf region off Concepción.

5. Conclusions

This study provides a first validation of MODIS-derived Chla in the river-influenced coastal upwelling system off central-southern Chile using a long in situ record from Station 18. The results show that default MODIS Chla captures the broad seasonal cycle of surface biomass, but systematically overestimates in situ Chla, particularly during periods when river discharge and coastal turbidity are enhanced. This positive bias is consistent with the optical complexity of river-influenced coastal waters, where CDOM, suspended particulate matter, atmospheric-correction uncertainty, and seasonal changes in phytoplankton community structure can modify the spectral signal used by standard blue-green Chla algorithms.

Among the raw satellite products tested here, 1-day MODIS Chla matchups produced the best agreement with in situ observations, whereas longer temporal composites substantially increased data availability at the cost of lower correspondence. MODIS nFLH showed more stable behavior across composite lengths, suggesting that it may serve as a useful complementary indicator of phytoplankton variability, although it does not fully resolve high Chla conditions. Therefore, nFLH should not be interpreted as a direct substitute for locally validated Chla retrievals, but rather as an independent fluorescence-based diagnostic to evaluate the consistency of high satellite Chla values in optically complex waters.

The machine-learning analysis further shows that MODIS reflectance data can be used to improve Chla estimates compared with the default MODIS product in the available Station 18 matchup dataset. This result supports the development of regionally tuned correction schemes for optically complex coastal waters influenced by river plumes. However, because the GBM model was evaluated using cross-validation rather than an independent spatially or temporally blocked validation dataset, the machine-learning results should be interpreted as a local proof of concept rather than a fully validated regional algorithm.

Overall, the results support the need for locally tuned correction schemes for river-influenced coastal waters off central-southern Chile, while also showing that any machine-learning-based regional Chla algorithm will require independent spatially distributed validation before it can be used operationally or generalized beyond the shelf region off Concepción. Future work should combine spatially distributed in situ Chla measurements, direct bio-optical observations, improved atmospheric-correction strategies, seasonally stratified validation, and independent matchup datasets to develop a robust regional coastal Chla algorithm for central-southern Chile.

Author Contributions: Conceptualization, G.S.S. and C.L.; methodology, G.S.S., R.M. and R.A.-G.; formal analysis, R.M., R.A.-G. and G.S.S.; investigation, G.S.S. and C.L.; resources, G.S.S. and F.J.T.; data curation, R.M.; writing—original draft preparation, G.S.S., R.A.-G., C.L., A.G. and F.J.T.; writing—review and editing, G.S.S., R.M., R.A.-G., A.G. and F.J.T. All authors have read and agreed to the published version of the manuscript.

Funding: Gonzalo Saldías has been partially supported by ANID Fondecyt Regular 1220167 and COPAS Coastal ANID FB210021. Fabián Tapia has also been supported by COPAS Coastal ANID FB210021. Alexander Galán has been partially supported by ANID programs Coastal Social-Ecological Millennium Institute (SECOS), Millennium Science Initiative ICN2019_015, and Concurso de Fortalecimiento al Desarrollo Científico de Centros Regionales 2020- R20F0008. The in situ measurements at Station 18 were funded by the Center for Oceanographic Research in the eastern South Pacific (FONDAP-COPAS Center, Research Grant No. 150100007) at Universidad de Concepción.

Data Availability Statement: Data from the in situ Chla and hydrographic observations at Station 18 are available upon request to the corresponding author, and will be available for direct download in late 2026.

Acknowledgments: We thank the Ocean Biology Processing Group (Code 614.2) at the GSFC, Greenbelt, MD 20771, for the production and distribution of the ocean color data. We thank the Oceanography Department at Universidad de Concepción for granting access to the 2002–2011 hydrographic data from Station 18.

Conflicts of Interest: The authors declare no conflicts of interest.

References

1. Shutler, J.D.; Quartly, G.D.; Donlon, C.J.; Sathyendranath, S.; Platt, T.; Chapron, B.; Johannessen, J.A.; Girard-Ardhuin, F.; Nightingale, P.D.; Woolf, D.K.; et al. Progress in satellite remote sensing for studying physical processes at the ocean surface and its borders with the atmosphere and sea ice. *Prog. Phys. Geogr.* **2016**, *40*, 215–246. [CrossRef]
2. McClain, C.R. A decade of satellite ocean color observations. *Annu. Rev. Mar. Sci.* **2009**, *1*, 19–42. [CrossRef]
3. Platt, T.; Sathyendranath, S. Oceanic primary production: Estimation by remote sensing at local and regional scales. *Science* **1988**, *241*, 1613–1620. [CrossRef] [PubMed]
4. Behrenfeld, M.J.; O'Malley, R.T.; Siegel, D.A.; McClain, C.R.; Sarmiento, J.L.; Feldman, G.C.; Milligan, A.J.; Falkowski, P.G.; Letelier, R.M.; Boss, E.S. Climate-driven trends in contemporary ocean productivity. *Nature* **2006**, *444*, 752–755. [CrossRef] [PubMed]
5. Brewin, R.J.; Tilstone, G.H.; Jackson, T.; Cain, T.; Miller, P.I.; Lange, P.K.; Misra, A.; Airs, R.L. Modelling size-fractionated primary production in the Atlantic Ocean from remote sensing. *Prog. Oceanogr.* **2017**, *158*, 130–149. [CrossRef]
6. Garcia, C.A.E.; Garcia, V.M.T.; McClain, C.R. Evaluation of SeaWiFS chlorophyll algorithms in the Southwestern Atlantic and Southern Oceans. *Remote Sens. Environ.* **2005**, *95*, 125–137.
7. Gregg, W.W.; Casey, N.W. Global and regional evaluation of the SeaWiFS chlorophyll data set. *Remote Sens. Environ.* **2004**, *93*, 463–479.
8. Yoder, J.A.; McClain, C.R.; Feldman, G.C.; Esaias, W.E. Annual cycles of phytoplankton chlorophyll concentrations in the global ocean: A satellite view. *Glob. Biogeochem. Cycles* **1993**, *7*, 181–193. [CrossRef]
9. Antoine, D.; André, J.M.; Morel, A. Oceanic primary production: 2. Estimation at global scale from satellite (coastal zone color scanner) chlorophyll. *Glob. Biogeochem. Cycles* **1996**, *10*, 57–69. [CrossRef]
10. Chavez, F.P. A comparison of ship and satellite chlorophyll from California and Peru. *J. Geophys. Res. Oceans (1978–2012)* **1995**, *100*, 24855–24862. [CrossRef]
11. Gregg, W.W.; Conkright, M.E. Global seasonal climatologies of ocean chlorophyll: Blending *in situ* and satellite data for the Coastal Zone Color Scanner era. *J. Geophys. Res. Oceans (1978–2012)* **2001**, *106*, 2499–2515. [CrossRef]

12. Thomas, A.C.; Strub, P.T.; Carr, M.E.; Weatherbee, R. Comparisons of chlorophyll variability between the four major global eastern boundary currents. *Int. J. Remote Sens.* **2004**, *25*, 1443–1447. [CrossRef]
13. Romero, S.I.; Piola, A.R.; Charo, M.; Garcia, C.A.E. Chlorophyll-a variability off Patagonia based on SeaWiFS data. *J. Geophys. Res. Oceans (1978–2012)* **2006**, *111*, C05021.
14. Hu, C.; Lee, Z.; Franz, B. Chlorophyll *a* algorithms for oligotrophic oceans: A novel approach based on three-band reflectance difference. *J. Geophys. Res. Oceans (1978–2012)* **2012**, *117*, C01011.
15. Nieto, K.; Mélin, F. Variability of chlorophyll-a concentration in the Gulf of Guinea and its relation to physical oceanographic variables. *Prog. Oceanogr.* **2017**, *151*, 97–115. [CrossRef] [PubMed]
16. Park, K.A.; Cha, N.Y.; Jeong, K.Y.; Byun, D.S.; Choi, B.J.; Lee, J.S. Long-term water types and satellite chlorophyll a variability in a river discharge environment around Ieodo Ocean Research Station. *Sci. Rep.* **2025**, *15*, 28240. [CrossRef] [PubMed]
17. Franz, B.A.; Werdell, P.J.; Meister, G.; Bailey, S.W.; Eplee, R.E., Jr.; Feldman, G.C.; Kwiatkowska, E.; McClain, C.R.; Patt, F.S.; Thomas, D. The continuity of ocean color measurements from SeaWiFS to MODIS. In *Proceedings of the Optics & Photonics 2005*; International Society for Optics and Photonics: Bellingham, WA, USA, 2005; p. 58820W.
18. O'Reilly, J.E.; Maritorena, S.; Mitchell, B.G.; Siegel, D.A.; Carder, K.L.; Garver, S.A.; Kahru, M.; McClain, C. Ocean color chlorophyll algorithms for SeaWiFS. *J. Geophys. Res. Oceans (1978–2012)* **1998**, *103*, 24937–24953. [CrossRef]
19. Franz, B.A.; Werdell, P.J.; Meister, G.; Kwiatkowska, E.J.; Bailey, S.W.; Ahmad, Z.; McClain, C.R. MODIS land bands for ocean remote sensing applications. In Proceedings of the Ocean Optics XVIII, Montreal, QC, Canada, 9–13 October 2006.
20. Gitelson, A.A.; Schalles, J.F.; Hladik, C.M. Remote chlorophyll-*a* retrieval in turbid, productive estuaries: Chesapeake Bay case study. *Remote Sens. Environ.* **2007**, *109*, 464–472. [CrossRef]
21. Le, C.; Li, Y.; Zha, Y.; Sun, D.; Huang, C.; Lu, H. A four-band semi-analytical model for estimating chlorophyll a in highly turbid lakes: The case of Taihu Lake, China. *Remote Sens. Environ.* **2009**, *113*, 1175–1182.
22. Chen, J.; Quan, W. An improved algorithm for retrieving chlorophyll-a from the Yellow River Estuary using MODIS imagery. *Environ. Monit. Assess.* **2013**, *185*, 2243–2255. [PubMed]
23. Le, C.; Hu, C.; Cannizzaro, J.; English, D.; Muller-Karger, F.; Lee, Z. Evaluation of chlorophyll-a remote sensing algorithms for an optically complex estuary. *Remote Sens. Environ.* **2013**, *129*, 75–89. [CrossRef]
24. Werdell, P.J.; Bailey, S.W.; Franz, B.A.; Harding Jr., L.W.; Feldman, G.C.; McClain, C.R. Regional and seasonal variability of chlorophyll-a in Chesapeake Bay as observed by SeaWiFS and MODIS-Aqua. *Remote Sens. Environ.* **2009**, *113*, 1319–1330.
25. Gholizadeh, H.; Robeson, S.M. Revisiting empirical ocean-colour algorithms for remote estimation of chlorophyll-a content on a global scale. *Int. J. Remote Sens.* **2016**, *37*, 2682–2705.
26. Siswanto, E.; Tang, J.; Yamaguchi, H.; Ahn, Y.H.; Ishizaka, J.; Yoo, S.; Kim, S.W.; Kiyomoto, Y.; Yamada, K.; Chiang, C.; et al. Empirical ocean-color algorithms to retrieve chlorophyll-a, total suspended matter, and colored dissolved organic matter absorption coefficient in the Yellow and East China Seas. *J. Oceanogr.* **2011**, *67*, 627–650.
27. Hu, C.; Carder, K.L.; Muller-Karger, F.E. Atmospheric correction of SeaWiFS imagery over turbid coastal waters: A practical method. *Remote Sens. Environ.* **2000**, *74*, 195–206.
28. Wang, M.; Shi, W. The NIR-SWIR combined atmospheric correction approach for MODIS ocean color data processing. *Opt. Express* **2007**, *15*, 15722–15733. [CrossRef] [PubMed]
29. Gower, J. A simpler picture of satellite chlorophyll fluorescence. *Remote Sens. Lett.* **2014**, *5*, 583–589. [CrossRef]
30. Lara, C.; Saldías, G.S.; Westberry, T.K.; Behrenfeld, M.J.; Broitman, B.R. First assessment of MODIS satellite ocean color products (OC3 and nFLH) in the Inner Sea of Chiloé, northern Patagonia. *Lat. Am. J. Aquat. Res.* **2017**, *45*, 822–827. [CrossRef]
31. Saldías, G.S.; Shearman, R.K.; Barth, J.A.; Tufillaro, N. Optics of the offshore Columbia River plume from glider observations and satellite imagery. *J. Geophys. Res. Oceans* **2016**, *121*, 2367–2384. [CrossRef]
32. Vásquez, S.I.; de la Torre, M.B.; Saldías, G.S.; Montecinos, A. Meridional changes in satellite chlorophyll and fluorescence in optically-complex coastal waters of northern Patagonia. *Remote Sens.* **2021**, *13*, 1026. [CrossRef]
33. Behrenfeld, M.J.; Westberry, T.; Boss, E.; O'malley, R.; Siegel, D.; Wiggert, J.D.; Franz, B.; McClain, C.; Feldman, G.; Doney, S.; et al. Satellite-detected fluorescence reveals global physiology of ocean phytoplankton. *Biogeosciences* **2009**, *6*, 779–794. [CrossRef]
34. Roesler, C.S.; Barnard, A.H. Optical proxy for phytoplankton biomass in the absence of photophysiology: Rethinking the absorption line height. *Methods Oceanogr.* **2013**, *7*, 79–94. [CrossRef]
35. Kwon, Y.S.; Baek, S.H.; Lim, Y.K.; Pyo, J.; Ligaray, M.; Park, Y.; Cho, K.H. Monitoring coastal chlorophyll-a concentrations in coastal areas using machine learning models. *Water* **2018**, *10*, 1020. [CrossRef]
36. Yuras, G.; Ulloa, O.; Hormazábal, S. On the annual cycle of coastal and open ocean satellite chlorophyll off Chile (18°–40° S). *Geophys. Res. Lett.* **2005**, *32, L23604*.
37. Morales, C.E.; González, H.E.; Hormazabal, S.E.; Yuras, G.; Letelier, J.; Castro, L.R. The distribution of chlorophyll-a and dominant planktonic components in the coastal transition zone off Concepción, central Chile, during different oceanographic conditions. *Prog. Oceanogr.* **2007**, *75*, 452–469. [CrossRef]

38. Corredor-Acosta, A.; Morales, C.E.; Brewin, R.J.W.; Auger, P.A.; Pizarro, O.; Hormazabal, S.; Anabalón, V. Phytoplankton Size Structure in Association with Mesoscale Eddies off Central-Southern Chile: The Satellite Application of a Phytoplankton Size-Class Model. *Remote Sens.* **2018**, *10*, 834.
39. Saldías, G.S.; Sobarzo, M.; Largier, J.; Moffat, C.; Letelier, R. Seasonal variability of turbid river plumes off central Chile based on high-resolution MODIS imagery. *Remote Sens. Environ.* **2012**, *123*, 220–233. [CrossRef]
40. Saldías, G.S.; Largier, J.L.; Mendes, R.; Pérez-Santos, I.; Vargas, C.A.; Sobarzo, M. Satellite-measured interannual variability of turbid river plumes off central-southern Chile: Spatial patterns and the influence of climate variability. *Prog. Oceanogr.* **2016**, *146*, 212–222.
41. Masotti, I.; Aparicio-Rizzo, P.; Yevenes, M.A.; Garreaud, R.; Belmar, L.; Farías, L. The influence of river discharge on nutrient export and phytoplankton biomass off the central Chile Coast (33°–37° S): Seasonal cycle and interannual variability. *Front. Mar. Sci.* **2018**, *5*, 423.
42. D'Sa, E.J.; Miller, R.L. Bio-optical properties in waters influenced by the Mississippi River during low flow conditions. *Remote Sens. Environ.* **2003**, *84*, 538–549. [CrossRef]
43. Le, C.; Lehrter, J.C.; Hu, C.; Murrell, M.C.; Qi, L. Spatiotemporal chlorophyll-a dynamics on the Louisiana continental shelf derived from a dual satellite imagery algorithm. *J. Geophys. Res. Oceans* **2014**, *119*, 7449–7462.
44. Minu, P.; Lotliker, A.A.; Shaju, S.; SanthoshKumar, B.; Ashraf, P.M.; Meenakumari, B. Effect of optically active substances and atmospheric correction schemes on remote-sensing reflectance at a coastal site off Kochi. *Int. J. Remote Sens.* **2014**, *35*, 5434–5447. [CrossRef]
45. Stuart, V.; Ulloa, O.; Alarcón, G.; Sathyendranath, S.; Major, H.; Head, E.J.; Platt, T. Bio-optical characteristics of phytoplankton populations in the upwelling system off the coast of Chile. *Rev. Chil. Hist. Nat.* **2004**, *77*, 87–105. [CrossRef]
46. Iriarte, J.L.; Vargas, C.A.; Tapia, F.J.; Bermúdez, R.; Urrutia, R.E. Primary production and plankton carbon biomass in a river-influenced upwelling area off Concepción, Chile. *Prog. Oceanogr.* **2012**, *92*, 97–109. [CrossRef]
47. Jacob, B.G.; Tapia, F.J.; Quiñones, R.A.; Montes, R.; Sobarzo, M.; Schneider, W.; Daneri, G.; Morales, C.E.; Montero, P.; González, H.E. Major changes in diatom abundance, productivity, and net community metabolism in a windier and dryer coastal climate in the southern Humboldt Current. *Prog. Oceanogr.* **2018**, *168*, 196–209. [CrossRef]
48. Daneri, G.; Dellarossa, V.; Quiñones, R.; Jacob, B.; Montero, P.; Ulloa, O. Primary production and community respiration in the Humboldt Current System off Chile and associated oceanic areas. *Mar. Ecol. Prog. Ser.* **2000**, *197*, 41–49. [CrossRef]
49. Sobarzo, M.; Bravo, L.; Donoso, D.; Garcés-Vargas, J.; Schneider, W. Coastal upwelling and seasonal cycles that influence the water column over the continental shelf off central Chile. *Prog. Oceanogr.* **2007**, *75*, 363–382. [CrossRef]
50. Muñoz, R.; Vergara, O.A.; Figueroa, P.A.; Mardones, P.; Sobarzo, M.; Saldías, G.S. On the phenology of coastal upwelling off central-southern Chile. *Dyn. Atmos. Oceans* **2023**, *104*, 101405. [CrossRef]
51. Letelier, J.; Pizarro, O.; Nuñez, S. Seasonal variability of coastal upwelling and the upwelling front off central Chile. *J. Geophys. Res. Oceans (1978–2012)* **2009**, *114*, C12009. [CrossRef]
52. Correa-Ramirez, M.A.; Hormazábal, S.; Yuras, G. Mesoscale eddies and high chlorophyll concentrations off central Chile (29°–39° S). *Geophys. Res. Lett.* **2007**, *34*, L12604.
53. Wang, M. Remote sensing of ocean contributions from ultraviolet to near-infrared using the shortwave infrared bands: Simulations. *Appl. Opt.* **2007**, *46*, 1535–1547. [CrossRef] [PubMed]
54. Bailey, S.W.; Werdell, P.J. A multi-sensor approach for the on-orbit validation of ocean color satellite data products. *Remote Sens. Environ.* **2006**, *102*, 12–23.
55. Hu, C.; Carder, K.L.; Muller-Karger, F.E. How precise are SeaWiFS ocean color estimates? Implications of digitization-noise errors. *Remote Sens. Environ.* **2001**, *76*, 239–249.
56. Stroh, J.; Panteleev, G.; Kirillov, S.; Makhotin, M.; Shakhova, N. Sea-surface temperature and salinity product comparison against external in situ data in the Arctic Ocean. *J. Geophys. Res. Oceans* **2015**, *120*, 7223–7236.
57. An, G.; Xing, M.; He, B.; Liao, C.; Huang, X.; Shang, J.; Kang, H. Using machine learning for estimating rice chlorophyll content from in situ hyperspectral data. *Remote Sens.* **2020**, *12*, 3104. [CrossRef]
58. Cao, Z.; Ma, R.; Duan, H.; Pahlevan, N.; Melack, J.; Shen, M.; Xue, K. A machine learning approach to estimate chlorophyll-a from Landsat-8 measurements in inland lakes. *Remote Sens. Environ.* **2020**, *248*, 111974. [CrossRef]
59. Vabalas, A.; Gowen, E.; Poliakoff, E.; Casson, A.J. Machine learning algorithm validation with a limited sample size. *PLoS ONE* **2019**, *14*, e0224365. [CrossRef] [PubMed]
60. Su, H.; Lu, X.; Chen, Z.; Zhang, H.; Lu, W.; Wu, W. Estimating coastal chlorophyll-a concentration from time-series OLCI data based on machine learning. *Remote Sens.* **2021**, *13*, 576.
61. Yao, H.; Huang, Y.; Wei, Y.; Zhong, W.; Wen, K. Retrieval of chlorophyll-a concentrations in the coastal waters of the Beibu Gulf in Guangxi using a gradient-boosting decision tree model. *Appl. Sci.* **2021**, *11*, 7855.

62. Oliveira Santos, V.; Guimarães, B.M.D.M.; Neto, I.E.L.; de Souza Filho, F.d.A.; Costa Rocha, P.A.; Thé, J.V.G.; Gharabaghi, B. Chlorophyll-a estimation in 149 tropical semi-arid reservoirs using remote sensing data and six machine learning methods. *Remote Sens.* **2024**, *16*, 1870.
63. Montecino, V.; Astoreca, R.; Alarcón, G.; Retamal, L.; Pizarro, G. Bio-optical characteristics and primary productivity during upwelling and non-upwelling conditions in a highly productive coastal ecosystem off central Chile (∼36° S). *Deep. Sea Res. Part II Top. Stud. Oceanogr.* **2004**, *51*, 2413–2426.
64. Anabalón, V.; Morales, C.; González, H.; Menschel, E.; Schneider, W.; Hormazabal, S.; Valencia, L.; Escribano, R. Micro-phytoplankton community structure in the coastal upwelling zone off Concepción (central Chile): Annual and inter-annual fluctuations in a highly dynamic environment. *Prog. Oceanogr.* **2016**, *149*, 174–188.
65. Sanchez, G.; Pantoja, S.; Lange, C.; Daneri, G. Seasonal changes in particulate biogenic and lithogenic silica in the upwelling system off Concepción (36° S), Chile, and their relationship to fluctuations in marine productivity and continental input. *Cont. Shelf Res.* **2008**, *28*, 2594–2600.
66. Testa, G.; Masotti, I.; Farías, L. Temporal Variability in Net Primary Production in an Upwelling Area off Central Chile (36° S). *Front. Mar. Sci.* **2018**, *5*, 8–24.
67. Anabalón, V.; Morales, C.; Escribano, R.; Varas, M.A. The contribution of nano-and micro-planktonic assemblages in the surface layer (0–30 m) under different hydrographic conditions in the upwelling area off Concepción, central Chile. *Prog. Oceanogr.* **2007**, *75*, 396–414.
68. Sezginer, Y.; Campbell, D.; Pillai, S.; Tortell, P. Fluorescence-based primary productivity estimates are influenced by non-photochemical quenching dynamics in Arctic phytoplankton. *Front. Microbiol.* **2023**, *14*, 1294521. [PubMed]
69. Falkowski, P.; Kolber, Z. Variations in chlorophyll fluorescence yields in phytoplankton in the world oceans. *Aust. J. Plant Physiol.* **1995**, *22*, 341–355. [CrossRef]
70. Binding, C.E.; Jerome, J.H.; Bukata, R.P.; Booty, W.G. Spectral absorption properties of dissolved and particulate matter in Lake Erie. *Remote Sens. Environ.* **2008**, *112*, 1702–1711. [CrossRef]
71. Shi, W.; Wang, M. An assessment of the black ocean pixel assumption for MODIS SWIR bands. *Remote Sens. Environ.* **2009**, *113*, 1587–1597. [CrossRef]
72. Garcia-Santos, Y.; Narváez, D.A.; Saldías, G.S.; Jacques-Coper, M.; Bozkurt, D.; Garreaud, R.; Valdés-Castro, V. Impact of atmospheric rivers on coastal oceanographic conditions off central-southern Chile. *Sci. Rep.* **2025**, *15*, 34569. [CrossRef] [PubMed]
73. Díaz-Astudillo, M.; Castillo, M.I.; Figueroa, P.A.; Castro, L.R.; Riquelme-Bugueño, R.; Pérez-Santos, I.; Pizarro, O.; Saldías, G.S. Cross-canyon variability in zooplankton backscattering strength in a river-influenced upwelling area. *Ocean Sci.* **2025**, *21*, 1833–1848.
74. Galán, A.; Sobarzo, M.; Saldías, G.S.; Curra-Sánchez, E.; Aguilera, V.M.; Manriquez, V.; Araneda, A.; Vargas, C.A. Riverine particulate organic matter exported to the adjacent coastal ocean: Implications for marine zooplankton in a highly productive coastal upwelling area. *J. Geophys. Res. Biogeosci.* **2026**, *131*, e2025JG008810. [CrossRef]

https://doi.org/10.3390/oceans7040059